Probing the Water Stability Limits and Degradation Pathways of Metal–Organic Frameworks

Mohamed E. A. Safy,[a] Muhamed Amin,[b] Rana R. Haikal,[a] Basma Elshazly,[a] Junjun Wang,[c] Yuemin Wang,[c] Christof Wöll,[c] and Mohamed H. Alkordi*[a]

Abstract: A comprehensive model to describe the water stability of prototypical metal–organic frameworks (MOFs) is derived by combining different types of theoretical and experimental approaches. The results provide an insight into the early stages of water-triggered destabilization of MOFs and allow detailed pathways to be proposed for the degradation of different MOFs under aqueous conditions. The essential elements of the approach are computing the pK_a values of coordinated water molecules and geometry relaxations. Variable-temperature and pH infrared spectroscopy techniques are used to corroborate the main findings. The model developed herein helps to explain stability limits observed for several prototypical MOFs, including MOF-5, HKUST-1, UiO-66, and MIL-101-Cr, in aqueous solutions, and thus, provides an insight into the possible degradation pathways in acidic and basic environments. The formation of a metal hydroxide through the autoprotolysis of metal-coordinated water molecules and the strength of carboxylate–metal interactions are suggested to be two key players that govern stability in basic and acidic media, respectively. The methodology presented herein can effectively guide future efforts, which are especially significant for in silico screening, for developing novel MOFs with enhanced aqueous stability.

Introduction

The large family of porous crystalline coordination polymers, commonly known as metal–organic frameworks (MOFs),[1,2] has attracted considerable scientific interest, since the first reports describing their permanent porosity against complete guest removal.[2] The hybrid composition of MOFs and myriad of available organic linkers and metal ions opened up an unlimited number of possibilities to arrive at scaffold materials tailored to specific applications, such as gas storage and separation,[2–4] CO_2 capture,[5] sensing,[6] catalysis,[7] water harvesting[8] and treatment,[9] and battery separators.[10,11] Despite unparalleled potential, aqueous structural stability limitations have precluded the widespread industrial utilization of MOFs, in general.[12]

[a] *M. E. A. Safy, Dr. R. R. Haikal, B. Elshazly, Prof. M. H. Alkordi*
Center for Materials Science
Zewail City of Science and Technology
October Gardens, Giza 12578 (Egypt)
E mail: malkordi@zewailcity.edu.eg

[b] *Dr. M. Amin*
Department of Sciences, University College Groningen
University of Groningen
9718 BG Groningen (Netherlands)

[c] *J. Wang, Dr. Y. Wang, Prof. C. Wöll*
Institute of Functional Interfaces (IFG)
Karlsruhe Institute of Technology (KIT)
Hermann von Helmholtz Platz 1
76344 Eggenstein Leopoldshafen (Germany)

Despite the plethora of water-stable MOFs reported, to date,[13] the vast majority suffer from structural degradation upon contact with aqueous media.[14] A fundamental understanding of the underlying chemical process(es) behind this phenomenon is therefore of high scientific interest. The emergence of water-stable MOFs, including UiO-66 and MIL-101, marked a turning point in the design and application of MOFs.[15,16] On the other extreme, the two prototypical MOFs, HKUST-1[17] and MOF-5,[18] featuring the copper acetate paddlewheel and the basic zinc acetate cluster, respectively, are highly prone to structural degradation if in contact with aqueous media.[14]

Our approach to probe this fundamental question includes the calculation of pK_a values of the metal-coordinated water molecules and metal-bridging hydroxides, in representative MOFs, based on classical electrostatic energies, which dominate the metal–ligand interactions in coordination compounds.[19] By combining structural relaxation of hydrated metal nodes and the variable-pH infrared spectroscopy investigations conducted herein, a comprehensive model was constructed to help explain the observed trends in the water susceptibility of a number of representative MOFs.

Experimental Section

General

Surface area measurements were conducted on an ASAP 2020 instrument by using N_2 isotherms; FTIR measurements were made on a ThermoScientific Nicolet-iS 10 spectrometer; all chemicals and

reagents were of commercial grade used without further purification. Acetonitrile for HPLC, gradient grade, $\geq$99.9%, and *N*,*N*-dimethylformamide (DMF) laboratory reagent grade purchased from Fischer. Copper(II) nitrate hemi(pentahydrate), $\geq$98% purity, $\leq$26% Cu basis purchased from Sigma Aldrich.

Synthesis of MOFs

Similar syntheses to previously reported procedures were conducted; the isolated MOF crystals were subsequently treated for activation, as also reported.[17]

FTIR analysis

For each MOF, a sample of about 10 mg was spread on filter paper, then a few drops of the aqueous solution (different pH each time) were dropped on top of the sample. The filter paper allowed quick drying of the solid sample to ensure brief exposure to the aqueous solution. The sample was maintained in contact with the added solution for 5 min, before being transferred to a glass vial for vacuum drying for 1 h prior to recording of its FTIR spectrum.

Computational methods

Cluster models of all studied MOFs were generated based on their crystal structures from the Cambridge Structural Database (CSD). The terminal acidic groups were neutralized by adding hydrogen atoms in the case of HKUST-1, UiO-66, and MIL-101-Cr. Because MOF-5 has no bridging hydroxyl group or coordinated water molecule to calculate its pK_a, one coordinated water molecule was added to the Zn cluster. All modeled clusters were optimized by using the B3LYP[20,21] functional and basis set of 6-31G + (d,p)[22] for C, O, N, and H atoms, as well as lanl2dz for all metals with effective core potentials. All quantum mechanical calculations were performed by using Gaussian 16 software.[23] Starting from the DFT-optimized structures, DELPHI was used to calculate the electrostatic energies between the metal, water molecules, hydroxides, oxo bridges, and organic ligands by solving the Poisson Boltzmann equation.[24] The partial charge distribution on the organic ligands was obtained from fitting the electrostatic potential in the DFT calculations. The metal ions and protic groups (water and oxo bridges) were parameterized, as described elsewhere.[19] Finally, the multiconformer continuum electrostatics (MCCE) program was used to calculate the Boltzmann distribution for the protonated and deprotonated states at different pH.[19,25] Linear interpolation was used to obtain pK_a, that is, the pH at which 50% of the protonated species was populated.

IRRAS data measurements

Infrared reflection absorption spectroscopy (IRRAS) data for the HKUST-1 MOF thin films were performed in a multitechnique ultrahigh vacuum (UHV) apparatus (Prevac, Poland). UHV-FTIR spectroscopy was used as the main technique.[26] All UHV-FTIR spectra were obtained by recording 1024 scans at a resolution of 4 cm ^{1} in reflectance mode. Dosing of D_2O was performed through a capillary tube ending in front of the sample. The temperature of the samples was monitored by a K-type thermocouple placed on the edge of the sample holder. Exposure to water was carried out at the indicated temperatures. All spectra shown were difference spectra obtained by subtracting a spectrum obtained immediately before exposure to water from that of the raw data.

Results and Discussion

Commonly proposed models for the observed stability of UiO-66, a MOF of Zr^{IV} ions bridged through carboxylate linkers, mostly revolve around the hard–soft acid–base (HSAB) model of interactions. According to this model, strong interactions between the Zr^{IV} ions, as a hard Lewis acid, and carboxylate oxygen atoms, as a hard Lewis base, are assumed.[13] Although this hypothesis is chemically sound, regarding the strong interactions commonly encountered in hard acid–hard base (HAHB) compounds, we propose an alternative postulate for the stability of this type of MOF and others.

Stability of UiO-66 and MIL-101

Although it is reasonable to assume strong interactions between high-valence cationic metal ions (e.g., Zr^{IV}, Ti^{IV}, Cr^{III}, and Al^{III}) and carboxylate ligands, this rather oversimplification of the complex situation in aqueous medium tends to overlook the formation of metal hydrates (M OH_2) upon contact of MOFs with water molecules. This generalization leads to an oversight of the commonly known formation of acidic hydrates of highly cationic metal ions in aqueous solution. Moreover, if the coordinated water molecules are sufficiently polarized (acidic), facilitating auto-deprotonation, even at neutral pH, the generated hydroxyl ions are expected to have stronger basic character than that of carboxylate ions. In such a scenario, the assumption of HAHB interactions in play is highly plausible, but it is the hydroxyl ions, with more localized negative charge, that should be regarded as the hard base, rather than the commonly postulated bridging or monodentate carboxylate ions, where charge delocalization is operative to a variable degree. Therefore, we propose that simply assigning the water stability of MOFs containing high-valence metal ions (best represented by UiO-66 and MIL-101) to HAHB interactions between carboxylate ions and high-valence metal cations is not an accurate model to capture the fundamentals for such observed water stability.

Our alternative proposed model for the stability/instability of MOFs in water is more comprehensive, in which balanced relative interactions are taken into consideration; these are mainly 1) the possible formation of metal hydrates, for which the pK_a values for such metal-coordinated water molecules are calculated; 2) speciation of bridging oxide/hydroxide ions in metal oxide/hydroxide clusters, whenever applicable; and 3) competition between carboxylate and hydroxyl ions towards binding metal cations.

If this model was applied to investigate the prominent stability of UiO-66, a MOF based on the metal oxide/hydroxide nodes $[Zr_6(\mu_3\text{-}O)_4(\mu_3\text{-}OH)_4(CO_2)_{12}]$, several interesting observations were made. The calculated pK_a values for the Zr-bridging oxygen species demonstrate rather interesting behavior (Figure 1 a), through which the bridging oxides tend to have a very low pK_a values, which indicate that they maintain a 2 formal charge over the whole range of pH from 0 to 14. However, the bridging hydroxyl ions demonstrated successive pK_a values (0, 2.3, 6, and 8.6). It is proposed herein that deprotona-

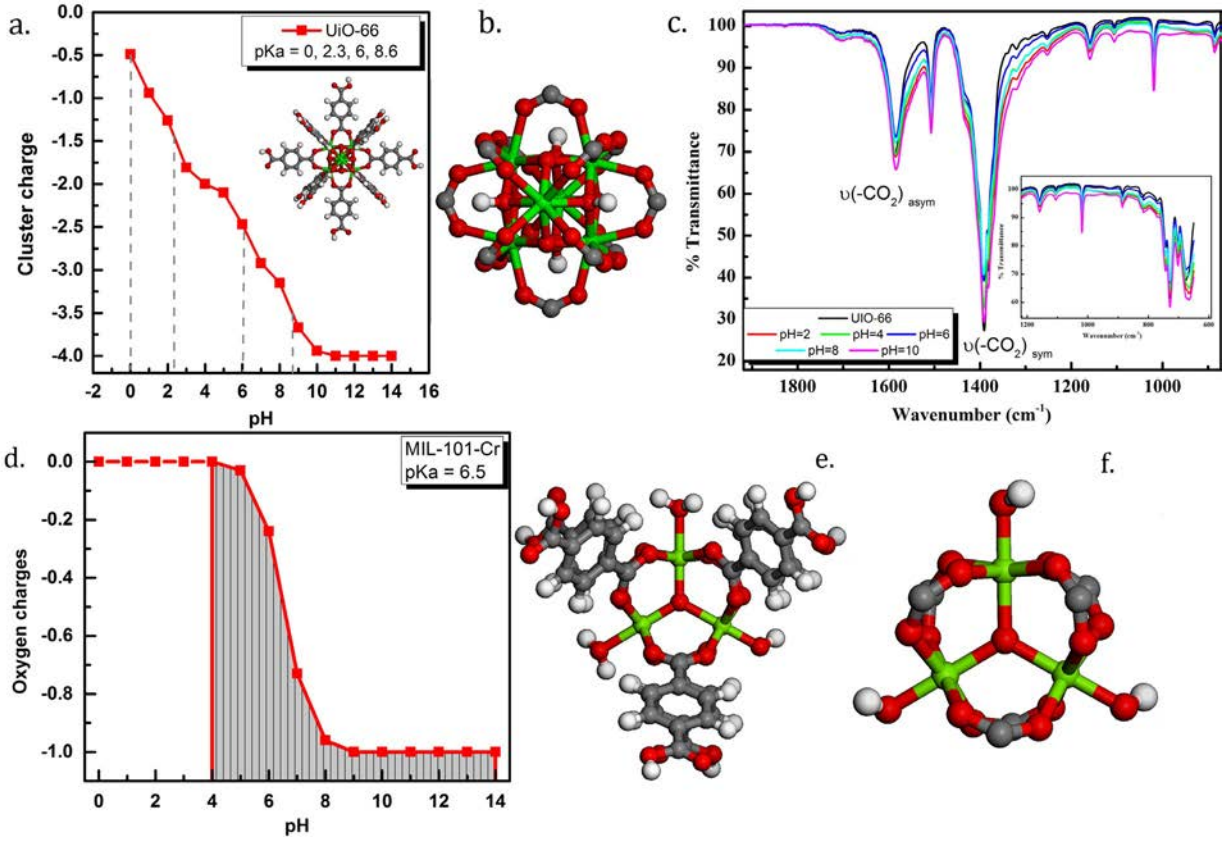

Figure 1. a) Calculated cluster charge and the corresponding pK_a values (dotted lines) for the four bridging hydroxyl ions in the $Zr_6(\mu_3\ O)_4(\mu_3\ OH)_4(CO_2)_{12}$ clusters in UiO 66 MOFs. b) Enlarged view of the geometry optimized Zr cluster. c) FTIR spectra for UiO 66 crystalline powder acquired after brief exposure to aqueous solution with variable pH values for 5 min at RT. d) Calculated charge as a function of pH on the Cr coordinated water molecules and the corresponding pK_a value. e) Geometry optimized hydrated Cr carboxylate cluster. f) Geometry optimized cluster coordinated by hydroxyl ions from deprotonated water molecules, showing the immediate environment around the Cr^{III} ions.

tion of the bridging hydroxyl ions in the Zr cluster does not lead to direct dissociation of the cluster, but rather to weakening of the interactions with the carboxylate linkers, as the cluster overall charge becomes less positive. In this regards, the Zr-cluster can be regarded as a priori hydroxylated species, making them more resistant to water hydrolysis. In line with pK_a calculations, we propose that UiO-66 hydrolysis in basic medium commences mainly through dissociation of the metal–carboxylate bonds, which is induced by a buildup of negative charge on the Zr oxide clusters. This proposed mechanism can be distinguished from a different model proposed above for hydrolysis of other MOFs with different cluster chemistry (those with open metal sites prone to water coordination). To probe this suggested model experimentally, FTIR spectra were collected for UiO-66 crystals after brief exposure to aqueous solutions with variable pH values (Figure 1 c). The C=O stretching band for the Zr-coordinated carboxylates ($\tilde{\nu}$ = 1584 cm^{-1}) does not demonstrate a significant change upon varying the pH of the solution; this indicates the kinetic stability of the MOF. This does not contradict a previous report on the loss of the crystallinity of UiO-66 immersed in a strong alkali solution for 2 h.[15] The observed kinetic stability of UiO-66 shown herein by probing the immediate microscopic environment of the Zr carboxylate clusters supports the proposed model for the structural degradation to proceed through gradual dissociation of the Zr carboxylate linkages due to accumulated negative charge on the Zr oxide cluster. It is due to the high connectivity (12-connected node) of the Zr carboxylate clusters that long-range structural integrity can still be maintained at solution pH exceeding the pK_a values calculated herein, and thus, imparting kinetic stability to UiO-66.

We note herein that several reports on the postsynthetic exchange (PSE) of organic linkers in UiO-66[27] and UiO-67[28] (based on the same Zr cluster) is readily accomplished with maintained structural integrity of the $Zr_6(\mu_3\text{-}O)_4(\mu_3\text{-}OH)_4(CO_2)_{12}$ clusters. This further supports the model suggested herein for the decomposition of the scaffold to be initiated through ligand dissociation from the $Zr_6(\mu_3\text{-}O)_4(\mu_3\text{-}OH)_4$ clusters, as facilitated by charge accumulation on the cluster due to deprotonation of Zr-bridging hydroxyl ions. The hydrolysis of UiO-66 in a highly acidic environment can be explained in terms of the reversible nature of metal–carboxylate coordination bonds, for which, in sufficiently acidic medium, the equilibrium is shifted to the formation of a free acid version of the linkers, and thus, facilitating framework degradation. We argue that this proposed explanation for UiO-66 instability in acidic medium can be generalized to other MOF families, for which the rate of hydrolysis and pH onset of structural degradation are highly de-

pendent on 1) the pK_a of the linker, 2) metal-ion valency, and 3) cluster connectivity (coordination number). In this model, a lower pK_a of the linker results in a higher valency of the metal ion, and a higher metal node connectivity results in greater resistance of the MOF to hydrolysis under acidic conditions.

The MIL-101 family of MOFs is based on the basic chromium acetate cluster, $[Cr_3(\mu_3\text{-}O)(H_2O)_2(OH)(CO_2)_6]$, which has demonstrated exceptional aqueous stability. The cluster is distinguished by a bridging μ_3-oxide at its core and six ditopic carboxylate linkers radiating from the Cr core in a trigonal prismatic geometry. The octahedral coordination geometry around each Cr^{III} ion is satisfied through coordination to a water molecule or a hydroxyl ion. The calculated pK_a for the Cr-coordinated water molecules was found to be 6.5 (Figure 1 d,e). This rather low pK_a value suggests that, even under neutral pH conditions, a significant percentage of the MIL-101-Cr clusters is expected to contain hydroxyl ions coordinated to the Cr metal sites, which impart anionic character to the framework in a neutral pH aqueous solution. This was indeed observed previously for MIL-101-Cr, the zeta-potential measurements of which indicated negative surface charge at pH > 6.[29] It is noted here that hydroxyl coordination to Cr ions did not adversely affect the cluster configuration (Figure 1 f), which suggested that deprotonation of coordinated water molecules mostly affected the overall charge on the cluster and not the Cr carboxylate/oxide connectivity. The negative-charge buildup on the Cr acetate cluster can destabilize the Cr carboxylate bonding by altering the charge density at the metal ions, and thus, weaken the electrostatic interactions with the linkers, providing a route for scaffold breakdown in neutral to basic media, similar to that proposed for UiO-66. The bond lengths in the geometry-optimized model of the MIL-101-Cr cluster (Figure 1 e) demonstrate a carboxylate–Cr bond of $d_{(Cr-O)} = 1.99$–2.01 Å, water coordination length of $d_{(Cr-OH_2)} = 2.12$–2.13 Å, and a bound hydroxyl ion length of $d_{(Cr-OH)} = 1.85$ Å. Upon deprotonation of the two water-coordinated molecules, the geometry-optimized structure indicated that the cluster stability was maintained with noticeable changes in bond length (Figure 1 f). A slight increase in the carboxylate–Cr bond length, $d_{(Cr-O)} = 2.01$–2.04 Å and bound hydroxyl ion distance $d_{(Cr-OH)} = 1.91$ Å were observed. Additionally, an increase in the distance of Cr O to the inner bridging oxide $d_{(Cr-O)} = 1.99$ Å was observed, compared with $d_{(Cr-O)} = 1.89$ Å in the pristine structure. Overall, these expansion in Cr O bond lengths are in line with the argument of weakened cluster stability due to the buildup of formal negative charge caused by metal-coordinated water deprotonation, which can lead down a cascade of metal–carboxylate dissociation. However, it is noted here that, due to the high valence and oxophilic nature of Cr^{III} ions, the fully deprotonated cluster still maintained structural integrity, similar to UiO-66. The mechanism of MOF degradation in acidic medium, similar to that proposed for UiO-66, is also assumed to be operative here. The high-valence Cr^{III} metal ion is expected to bind efficiently to the carboxylate anions, as expected from the HAHB principle, and only if the equilibrium is sensibly shifted towards decomposition products of the free carboxylic acid form can degradation of the MOF be observed.

Stability of HKUST-1 and MOF-5

Our focus herein is directed towards investigating the known instability of two widely known MOFs, HKUST-1 and MOF-5. We propose that degradation of the MOF structure in these two cases passes through an initial hydration step, involving coordination of water molecules to the metal ions. In the case of HKUST-1, axial water coordination to the Cu acetate paddlewheel is commonly known. For the basic zinc acetate cluster encountered in MOF-5, Zn^{II} hydration can occur if the tetrahedrally coordinated Zn^{II} ion expands its coordination number to form a distorted trigonal bipyramidal coordination sphere around the Zn^{II} ion.[30] In a subsequent step, auto-deprotonation of the metal-coordinated water molecule can readily form a metal hydroxide, which triggers a downhill pathway for restructuring of the metal carboxylate cluster, and hence, overall MOF degradation. It is therefore paramount to gain an insight into the pK_a of such metal-coordinated water molecules to better assess the significance of this proposed pathway.

Our results strongly indicate the facile formation of metal hydroxides upon metal hydration at moderate pH values for such soft metal ions. Zn^{II} and Cu^{II} are the most common node types in Zn acetate and Cu paddlewheels, respectively. In neutral to even slightly acidic solution, the formation of Cu OH^- from autoprotolysis of coordinated water molecules is expected, based on a calculated pK_a value of 6.2 for the Cu^{II}-coordinated water molecule (Figure 2 a). Additionally in aqueous solutions at pH > 4, considerable buildup of negative charge on Cu-coordinated water molecules is expected (Figure 2 a). The geometry-optimized structure of the Cu paddlewheel after formal deprotonation of one coordinated water molecule demonstrates major structural deformation relative to that of the initial structure (Figure 2 b). The two main observed changes were 1) dissociation of a Cu^{II}–carboxylate bond for Cu^{II} bearing the hydroxyl ion, and 2) induced structural changes in the coordination sphere around the second Cu^{II} ion where a square-planar coordination geometry was observed instead of the original square pyramidal configuration. The former change demonstrates one plausible pathway towards structural degradation of HKUST-1 in aqueous media, whereas the latter is particularly significant because it might help to explain certain observations made elsewhere, in which rapid deterioration of HKUST-1 performance as a microporous sorbent for certain gas molecules can be affected by exposure to moisture.[31] In fact, release of NO-adsorbed molecules on Cu^{II} sites can be triggered by contacting HKUST-1 with moisture.[32] The observation of retained crystallinity, but deteriorated adsorption performance, indicates the importance of not only considering long-range effect(s) on specific crystallinity of a MOs (as commonly probed through XRD studies), but also on focusing on localized effect(s) at/near the binding site(s).[33] The geometry-optimized structure of the hydrated Cu-paddlewheel unit in HKUST-1 demonstrated the following bond lengths: Cu–carboxylate of $d_{(Cu-O)} = 1.85$ Å, carboxylate C O $d_{(C-O)} = 1.21$ Å, and Cu OH_2 $d_{(Cu-O)} = 2.21$ Å. Upon deprotonation of one of the Cu-coordinated water molecules, dramatic changes to the paddlewheel structure were observed (Figure 2 b). The Cu–carboxyl-

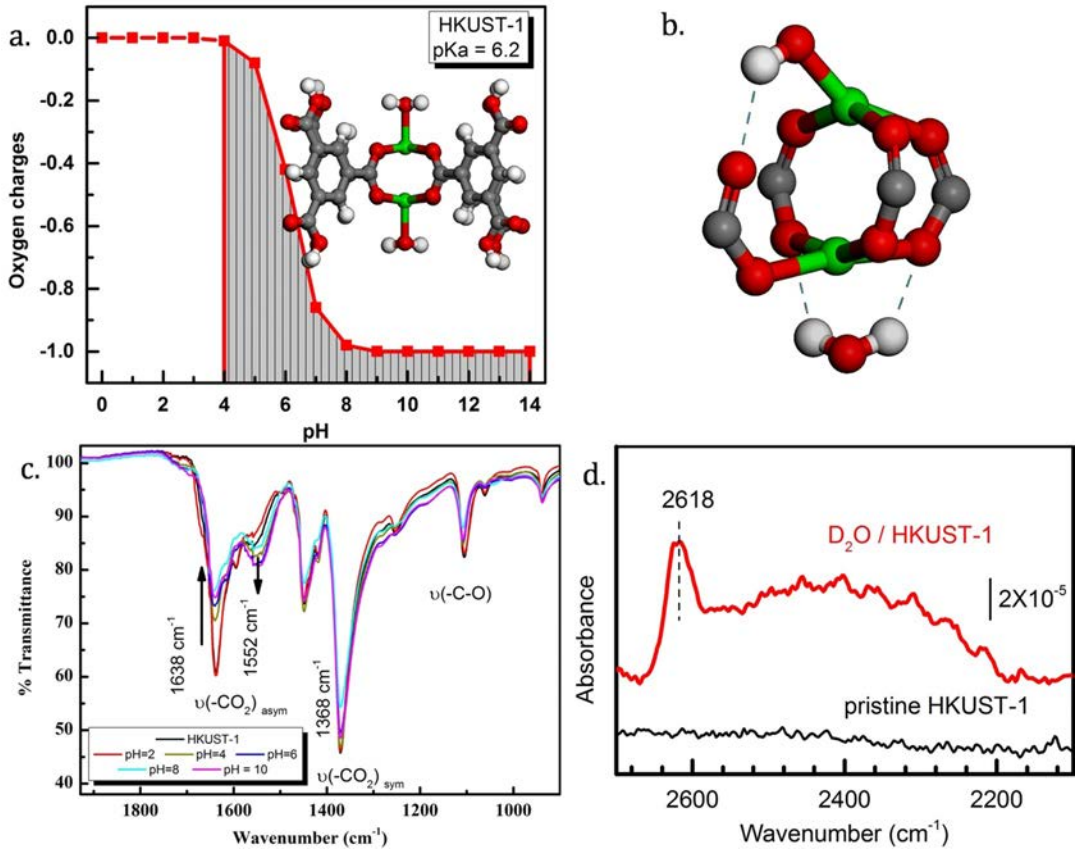

Figure 2. a) Calculated charge on the Cu^{II} coordinated water molecules in HKUST 1, and the calculated pK_a value; the inset shows the geometry optimized structure of the Cu^{II} paddlewheel cluster with coordinated water molecules. b) Geometry optimized structure after formal deprotonation of one water mole cule. The cleaved Cu carboxylate bond is indicated by an orange double headed arrow; hydrogen bonding is indicated by broken blue lines. c) FTIR spectra for the HKUST 1 crystalline powder acquired after brief exposure to an aqueous solution with variable pH values for 5 min at RT. d) IRRAS data measured under UHV conditions for hydrated HKUST 1 thin films by dosing D_2O at 200 K and subsequent annealing to 300 K. The IRRAS data are difference spectra ob tained by subtracting a reference spectrum recorded immediately for the HKUST 1 substrate before exposure to water.

ate $d_{(Cu–O)}$ bond lengths were significantly elongated (1.94–2.06 Å) for the hydroxyl-coordinated Cu ion, at which the coordinated hydroxyl ion became formally bound to the Cu ion, $d_{(Cu–O)} = 1.85$ Å.

Regarding the linkers, the carboxylate C O bond lengths did not change appreciably, $d_{(C–O)} = 1.27$ and 1.29 Å, indicating maintained charge delocalization in the carboxylate linkers, with the exception of the carboxylate ligand liberated from coordination to one of the Cu ions (substituted by the hydroxyl ion). In this particular ligand, two distinguishable C O bond lengths were observed, $d_{(C\ O)} = 1.26$ and 1.31 Å. The distinct C O bond order in this particular carboxylate ion is in agreement with its monodentate coordination configuration to one of the Cu ions (Figure 2b). Overall, the paddlewheel structure was not maintained upon deprotonation of one of the two Cu-coordinated water molecules; this signifies a potential pathway for metal-node decomposition in aqueous media. This observation is in line with the previously postulated model of degradation of HKUST-1, in which the oxidation state of the hydroxyl-bound Cu ion is argued to be Cu^{I}, as supported by EPR spectroscopy analysis.[34] However, we note that the decomposition step proposed here can be regarded as an intermediate in the decomposition pathway, resulting in the species shown by Todaro et al. to contain Cu^{I} ions.[34]

To probe the effect of solution pH on the Cu^{II}-paddlewheel structure, several FTIR spectra were recorded for the solid briefly exposed to aqueous solutions over a variable pH range (Figure 2c). The FTIR spectra demonstrate appreciable changes, specifically in the asymmetric C=O stretching mode at $\tilde{\nu} = 1638\ cm^{-1}$. This observation can be explained in terms of weakened or formally dissociated Cu^{II}–carboxylate bonds upon contact with an aqueous solution at pH > 4. The maintained FTIR spectral characteristics of the solid after immersion in aqueous solution at pH 2 is in good agreement with the results from pK_a calculations. Moreover, decay in the $\tilde{\nu} = 1638\ cm^{-1}$ band after treatment at pH > 4 was accompanied by a noticeable appearance of a vibrational band at $\tilde{\nu} = 1552\ cm^{-1}$, and a gradual increase in its relative intensity, which can be ascribed to the monodentate Cu-coordinated carboxylate stretching (marked band in Figure 2c).

IRRAS data recorded under UHV conditions for HKUST-1 thin films after dosing with D_2O provide an insight into water-induced changes. Exposing pristine HKUST-1 to D_2O at low temperatures (200 K) and gently heating to 300 K leads to the de-

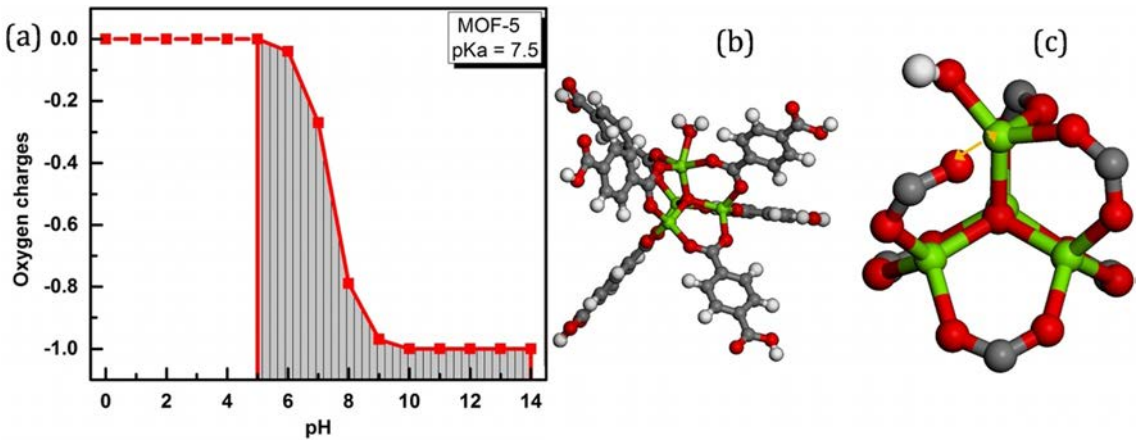

Figure 3. a) Calculated charge on the Zn^{II} coordinated water molecule in hydrated MOF 5 and the calculated pK_a value. b) Geometry optimized structure of the hydrated cluster. c) Geometry optimized structure of the basic Zn acetate cluster after formal deprotonation of the coordinated water molecule; the cleaved Zn carboxylate bond is indicated by an orange double headed arrow.

sorption of weakly bound water molecules, including multilayers adsorbed at the surface and D_2O clusters contained within the pores of HKUST-1. The IRRAS data show a narrow IR band at $\tilde{\nu} = 2618\ cm^{-1}$ (Figure 2d), which is stable at temperatures higher than 400 K. This band is assigned to OD species formed through deprotonation of D_2O molecules bound to Cu^{II} metal sites. The frequency of 2618 cm^{-1} is much lower than those of non-hydrogen-bonded OD species adsorbed at metal oxide surfaces (e.g., 2710 cm^{-1} for OD bound to Zn^{2+} ions on a ZnO surface).[35] This significant redshift reveals hydrogen-bonding interactions between Cu^{II}-coordinated OD species and adjacent framework carboxylate groups, in line with the DFT-optimized structure shown in Figure 2b. In addition, Figure 2d displays a broad feature at $\tilde{\nu} = 2560–2200\ cm^{-1}$ that is characteristic for hydrogen-bonded water molecules.[35] These intact D_2O molecules are stable at 300 K through the interaction with Cu^{II} sites and framework carboxylates. It should be noted that water clusters in the pores only yield weak perturbations of the paddlewheel units: a carboxylate band at $\tilde{\nu} \approx 1655\ cm^{-1}$. The changes are most significant for the fully hydrated sample at 200 K and decrease to a minimum after annealing to 300 K (data not shown). This observation is fully consistent with our model, which predicts substantial structural degradations of HKUST-1 only if the MOF is fully hydrated at 300 K,[36] with a pH of greater than 6.2.

Modeling the interaction(s) of MOF-5 with water molecules was conducted by hydrating one of the Zn^{II} ions in the basic Zn acetate cluster through water coordination (Figure 3). The calculated charge on the oxygen atom of the coordinated water molecule as a function of pH (Figure 3a) indicates a gradual buildup of formal negative charge at pH > 5, with pK_a = 7.5. This rather low value of calculated pK_a is in good agreement with commonly known instability of MOF-5 in aqueous solution. The coordination of one water molecule to a Zn^{II} ion induced structural deformation to the cluster; this is most pronounced at the water-coordinated Zn^{II} ion. The Zn–carboxylate bond length, $d_{(Zn–O)}$, changed from 2.0 to 2.12 Å, signifying weakening of the Zn–carboxylate bond upon water coordination (Figure 3b). This is in agreement with previous reports on the structure of hydrated MOF-5 node.[37,38] We propose that for a solution at pH > 4 degradation of MOF-5 is triggered through water coordination to Zn^{II} ions, which is followed by hydrolysis due to polarization of the coordinated water molecule by a Zn^{II} ion. Each generated hydroxyl ion, a stronger base than that of carboxylate, causes dissociation of one Zn–carboxylate bond (Figure 3c). The increased Zn–carboxylate bond lengths in the hydroxyl-coordinated Zn acetate cluster indicated significantly weakened Zn–carboxylate interactions, $d_{(Zn–O)}$, which changed from 2.02–2.12 Å in the solvated cluster to 2.23 Å in the deprotonated cluster.

Overall, the decomposition pathway proposed for MOF-5 and HKUST-1 assumingly proceeds through two consecutive steps: 1) coordination of a water molecule to the metal ion, weakening metal–carboxylate interactions, especially in closed-sphere metal complexes (e.g., MOF-5); and 2) deprotonation of the coordinated water at neutral to even slightly acidic aqueous environment, leading to formal metal–carboxylate bond dissociation. It is this latter effect that triggers a cascade of structural changes, leading to irreversible scaffold decomposition, loss of crystallinity, and diminished surface area.

Thermodynamic and kinetic stability limits

The findings presented so far indicate that a specific MOF can be thermodynamically stable at a relatively narrow range of solution pH. This thermodynamic stability range is flanked between an upper solution pH value at which coordinated water or deprotonation of bridging hydroxyl ions is sufficient to labilize metal–carboxylate bonds. The lower end of this stability range is determined by the metal–carboxylate association constant, which, in turn, reflects the generally accepted HAHB interaction principle (Scheme 1). It is worth mentioning that the latest attempts to selectively etch certain parts of MOFs by utilizing bulky acids, such as H_3PO_4, were made in aprotic solvents, such as DMF, which does not contradicting the general scheme proposed herein for the acid-triggered degradation of MOFs. The use of bulky acid molecules in aprotic solvent

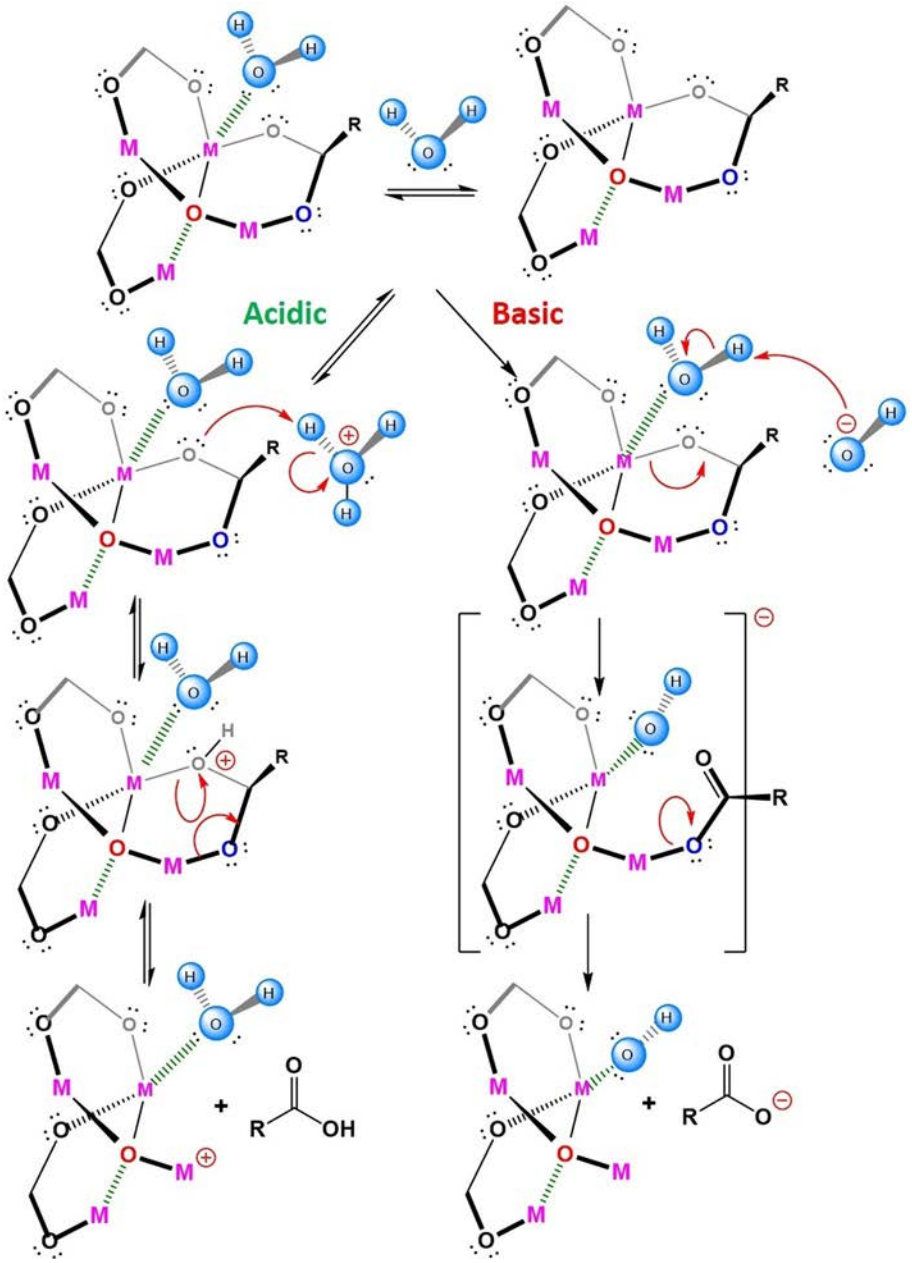

Scheme 1. Proposed degradation pathways under acidic and basic conditions for MOFs based on metal carboxylate clusters (a hypothetical metal carboxyl ate cluster is used here as an illustrative example, with which the basic principles shown in this model can be readily transferrable to other types of metal carboxylate MOFs). Metal ion hydration is assumed to be the initial stage in the process, followed by either ligand protonation (in acidic medium) or deproto nation of coordinated water molecule (neutron to basic medium). The strong interactions between metal ions and hydroxyl ions are assumed to cause irrever sible damage to the nodes of a particular MOF.

avoided the generation of hydronium ions, and thus, successfully attained the targeted selective itching of the MOF.[39]

We additionally note that a slightly expanded stability limit can exist, preferably described as the kinetic stability range, at which a specific MOF can still demonstrate transient structural stability. This stability range is highly dependent on the cluster connectivity number, solution temperature, and time of exposure to the acid/base. It is possible that transient structural damage to the MOF can be reversed within its kinetic stability limit, given that the microenvironment at the metal node is not significantly altered from the optimal geometry. As fundamental as such stability limits are for each type of MOF, and intimately related to its structure and connectivity, it becomes clear that an approach that can provide a physical barrier between water molecules and the metal–carboxylate clusters in MOFs merits investigation. Surface passivation, which has long been known to prevent the corrosion of metal and alloy surfaces, even under thermodynamically favored conditions, represents a highly relevant attempt to impart structural stability to MOFs under hydrolytic conditions. An immediately clear challenge arises, in which a physical barrier between the MOF and aqueous solution is sought, while simultaneously maintaining

accessibility to the pore system by gaseous and small molecules. Additionally, an approach that can be easily generalized and transferrable to different types of MOFs is of significance. Finally, due to drastically different synthetic conditions for the large number of known MOFs, a surface passivation approach that can be applied postsynthetically, utilizing relatively mild conditions, that is suitable for most of the known MOFs is of particular importance. As it becomes evident that the key to enhancing the water stability of MOFs over a wide pH range, while in contact with aqueous solution, is to form a protective passivation layer on the surface of the MOF crystallites. Indeed, several reports have outlined different tactics to improve the hydrostability of water-sensitive MOFs, especially HKUST-1.[40–42] The general concept is mainly directed towards rendering the MOF surface hydrophobic, in an attempt to enhance the resistance to moisture/water. This can be achieved through coating of the MOF, postsynthetically, with hydrophobic polymers.[41,43,44] Alternatively, the incorporation of hydrophobic graphite oxide during MOF synthesis has been shown to enhance the hydrothermal stability and catalytic activity of HKUST-1.[45] Confined crystallization of HKUST-1 within the mesopores of amine-functionalized silica has also been proven to maintain the structural integrity of the MOF crystallites in a humid environment due to the stable mesoporous solid support.[46]

Conclusion

A comprehensive model to explain the stability limits of carboxylate-based MOFs in an aqueous environment was developed. In this model, we identified two distinct mechanisms for MOF structural degradation in neutral to basic solutions, depending on the nature of the metal cluster (nodes). A common degradation pathway is suggested in an acidic environment that takes into consideration the strength of metal–carboxylate bonds, in line with the widely accepted HAHB model. It is the specific nature of each MOF, more specifically the valence of metal ions, and node chemistry that set the intrinsic thermodynamic stability limits for a particular MOF. In neutral to basic media, deprotonation of metal-coordinated water molecules appears to trigger a cascade of reactions, leading to structural degradation of such MOFs. Additionally, it is suggested that, even beyond the thermodynamic limit of stability, certain MOFs can still be considered kinetically inert; this is mostly due to the high connectivity of their metal–carboxylate nodes. The methodology presented herein can effectively be utilized in current MOF design approaches guided by in silico modeling of a target blueprint material, through which facile calculation of pK_a values of the metal-coordinated water molecules can be conducted a priori, to enhance lead selection and optimization towards water-stable MOFs.

Acknowledgements

We acknowledge financial support of this project from the Zewail City of Science and Technology (CMS-MA). We thank Dr. Ali Abdelrasool (Kuwait University) for helping with drawings of the reaction mechanism and Abhinav Chandresh (KIT) for providing the HKUST-1 MOF thin film.

Conflict of interest

The authors declare no conflict of interest.

Keywords: kinetics · hydrolysis · metal–organic frameworks · thermodynamics · water stability limits

[1] A. Kirchon, L. Feng, H. F. Drake, E. A. Joseph, H. C. Zhou, *Chem. Soc. Rev.* **2018**, *47*, 8611.
[2] H. Furukawa, K. E. Cordova, M. O'Keeffe, O. M. Yaghi, *Science* **2013**, *341*, 1230444.
[3] P. Nugent, Y. Belmabkhout, S. D. Burd, A. J. Cairns, R. Luebke, K. Forrest, T. Pham, S. Ma, B. Space, L. Wojtas, M. Eddaoudi, M. J. Zaworotko, *Nature* **2013**, *495*, 80.
[4] Y. Belmabkhout, P. M. Bhatt, K. Adil, R. S. Pillai, A. Cadiau, A. Shkurenko, G. Maurin, G. Liu, W. J. Koros, M. Eddaoudi, *Nat. Energy* **2018**, *3*, 1059.
[5] M. R. Tchalala, P. M. Bhatt, K. N. Chappanda, S. R. Tavares, K. Adil, Y. Bel mabkhout, A. Shkurenko, A. Cadiau, N. Heymans, G. De Weireld, G. Maurin, K. N. Salama, M. Eddaoudi, *Nat. Commun.* **2019**, *10*, 1328.
[6] I. Stassen, J. H. Dou, C. Hendon, M. Dincă, *ACS Cent. Sci.* **2019**, *5*, 1425.
[7] A. Dhakshinamoorthy, Z. Li, H. Garcia, *Chem. Soc. Rev.* **2018**, *47*, 8134.
[8] H. Kim, S. R. Rao, E. A. Kapustin, L. Zhao, S. Yang, O. M. Yaghi, E. N. Wang, *Nat. Commun.* **2018**, *9*, 1191.
[9] W. A. El Mehalmey, A. H. Ibrahim, A. A. Abugable, M. H. Hassan, R. R. Haikal, S. G. Karakalos, O. Zaki, M. H. Alkordi, *J. Mater. Chem. A* **2018**, *6*, 2742.
[10] M. Li, Y. Wan, J. K. Huang, A. H. Assen, C. E. Hsiung, H. Jiang, Y. Han, M. Eddaoudi, Z. Lai, J. Ming, L. J. Li, *ACS Energy Lett.* **2017**, *2*, 2362.
[11] S. Suriyakumar, A. M. Stephan, N. Angulakshmi, M. H. Hassan, M. H. Al kordi, *J. Mater. Chem. A* **2018**, *6*, 14623.
[12] A. J. Howarth, Y. Liu, P. Li, Z. Li, T. C. Wang, J. T. Hupp, O. K. Farha, *Nat. Rev. Mater.* **2016**, *1*, 15018.
[13] S. Yuan, J. S. Qin, C. T. Lollar, H. C. Zhou, *ACS Cent. Sci.* **2018**, *4*, 440.
[14] P. Küsgens, M. Rose, I. Senkovska, H. Fröde, A. Henschel, S. Siegle, S. Kaskel, *Microporous Mesoporous Mater.* **2009**, *120*, 325.
[15] M. Kandiah, M. H. Nilsen, S. Usseglio, S. Jakobsen, U. Olsbye, M. Tilset, C. Larabi, E. A. Quadrelli, F. Bonino, K. P. Lillerud, *Chem. Mater.* **2010**, *22*, 6632.
[16] G. Férey, C. Mellot Draznieks, C. Serre, F. Millange, J. Dutour, S. Surblé, I. Margiolaki, *Science* **2005**, *309*, 2040.
[17] S. S. Y. Chui, S. M. F. Lo, J. P. H. Charmant, A. G. Orpen, I. D. Williams, *Sci ence* **1999**, *283*, 1148.
[18] H. Li, M. Eddaoudi, M. O'Keeffe, O. M. Yaghi, *Nature* **1999**, *402*, 276.
[19] M. Amin, L. Vogt, S. Vassiliev, I. Rivalta, M. M. Sultan, D. Bruce, G. W. Brudvig, V. S. Batista, M. R. Gunner, *J. Phys. Chem. B* **2013**, *117*, 6217.
[20] A. D. Becke, *J. Chem. Phys.* **1993**, *98*, 5648.
[21] C. Lee, W. Yang, R. G. Parr, *Phys. Rev. B* **1988**, *37*, 785.
[22] R. Krishnan, J. S. Binkley, R. Seeger, J. A. Pople, *J. Chem. Phys.* **1980**, *72*, 650.
[23] Gaussian 16, Revision B.01, M. J. Frisch, G. W. Trucks, H. B. Schlegel, G. E. Scuseria, M. A. Robb, J. R. Cheeseman, G. Scalmani, V. Barone, G. A. Pe tersson, H. Nakatsuji, X. Li, M. Caricato, A. V. Marenich, J. Bloino, B. G. Ja nesko, R. Gomperts, B. Mennucci, H. P. Hratchian, J. V. Ortiz, A. F. Izmay lov, J. L. Sonnenberg, D. Williams Young, F. Ding, F. Lipparini, F. Egidi, J. Goings, B. Peng, A. Petrone, T. Henderson, D. Ranasinghe, V. G. Zakrzew ski, J. Gao, N. Rega, G. Zheng, W. Liang, M. Hada, M. Ehara, K. Toyota, R. Fukuda, J. Hasegawa, M. Ishida, T. Nakajima, Y. Honda, O. Kitao, H. Nakai, T. Vreven, K. Throssell, J. A. Montgomery, Jr., J. E. Peralta, F. Ogliaro, M. J. Bearpark, J. J. Heyd, E. N. Brothers, K. N. Kudin, V. N. Staro verov, T. A. Keith, R. Kobayashi, J. Normand, K. Raghavachari, A. P. Ren dell, J. C. Burant, S. S. Iyengar, J. Tomasi, M. Cossi, J. M. Millam, M. Klene, C. Adamo, R. Cammi, J. W. Ochterski, R. L. Martin, K. Morokuma, O. Farkas, J. B. Foresman, D. J. Fox, Gaussian Inc., Wallingford CT, **2016**.

[24] N. A. Baker, D. Sept, S. Joseph, M. J. Holst, J. A. McCammon, *Proc. Natl. Acad. Sci. USA* **2001**, *98*, 10037.
[25] Y. Song, J. Mao, M. R. Gunner, *J. Comput. Chem.* **2009**, *30*, 2231.
[26] Y. Wang, C. Wöll, *Chem. Soc. Rev.* **2017**, *46*, 1875.
[27] G. C. Shearer, J. G. Vitillo, S. Bordiga, S. Svelle, U. Olsbye, K. P. Lillerud, *Chem. Mater.* **2016**, *28*, 7190.
[28] J. E. Mondloch, M. J. Katz, N. Planas, D. Semrouni, L. Gagliardi, J. T. Hupp, O. K. Farha, *Chem. Commun.* **2014**, *50*, 8944.
[29] T. Chen, C. Zhang, Y. Qin, H. Yang, P. Zhang, F. Ye, *Materials* **2017**, *10*, 879.
[30] J. A. Greathouse, M. D. Allendorf, *J. Am. Chem. Soc.* **2006**, *128*, 10678.
[31] N. Al Janabi, P. Hill, L. Torrente Murciano, A. Garforth, P. Gorgojo, F. Siperstein, X. Fan, *Chem. Eng. J.* **2015**, *281*, 669.
[32] B. Xiao, P. S. Wheatley, X. Zhao, A. J. Fletcher, S. Fox, A. G. Rossi, I. L. Megson, S. Bordiga, L. Regli, K. M. Thomas, R. E. Morris, *J. Am. Chem. Soc.* **2007**, *129*, 1203.
[33] L. N. McHugh, M. J. McPherson, L. J. McCormick, S. A. Morris, P. S. Wheatley, S. J. Teat, D. McKay, D. M. Dawson, C. E. F. Sansome, S. E. Ashbrook, C. A. Stone, M. W. Smith, R. E. Morris, *Nat. Chem.* **2018**, *10*, 1096.
[34] M. Todaro, G. Buscarino, L. Sciortino, A. Alessi, F. Messina, M. Taddei, M. Ranocchiari, M. Cannas, F. M. Gelardi, *J. Phys. Chem. C* **2016**, *120*, 12879.
[35] C. Wöll, *ACS Catal.* **2020**, *10*, 168.
[36] K. Müller, N. Vankova, L. Schöttner, T. Heine, L. Heinke, *Chem. Sci.* **2019**, *10*, 153.
[37] Y. Ming, N. Kumar, D. J. Siegel, *ACS Omega* **2017**, *2*, 4921.
[38] M. De Toni, R. Jonchiere, P. Pullumbi, F. X. Coudert, A. H. Fuchs, *Chem PhysChem* **2012**, *13*, 3497.
[39] J. Koo, I. C. Hwang, X. Yu, S. Saha, Y. Kim, K. Kim, *Chem. Sci.* **2017**, *8*, 6799.
[40] M. Ding, X. Cai, H. L. Jiang, *Chem. Sci.* **2019**, *10*, 10209.
[41] W. Zhang, Y. Hu, J. Ge, H. L. Jiang, S. H. Yu, *J. Am. Chem. Soc.* **2014**, *136*, 16978.
[42] Z. R. Jiang, J. Ge, Y. X. Zhou, Z. U. Wang, D. Chen, S. H. Yu, H. L. Jiang, *NPG Asia Mater.* **2016**, *8*, e253.
[43] S. Yang, L. Peng, D. T. Sun, M. Asgari, E. Oveisi, O. Trukhina, S. Bulut, A. Jamali, W. L. Queen, *Chem. Sci.* **2019**, *10*, 4542.
[44] C. A. Fernandez, S. K. Nune, H. V. Annapureddy, L. X. Dang, B. P. McGrail, F. Zheng, E. Polikarpov, D. L. King, C. Freeman, K. P. Brooks, *Dalton Trans.* **2015**, *44*, 13490.
[45] D. D. Zu, L. Lu, X. Q. Liu, D. Y. Zhang, L. B. Sun, *J. Phys. Chem. C* **2014**, *118*, 19910.
[46] M. Mazaj, T. Čendak, G. Buscarino, M. Todaro, N. Zabukovec Logar, *J. Mater. Chem. A* **2017**, *5*, 22305.